Hindawi
Journal of Chemistry
Volume 2022, Article ID 3567606, 11 pages
https://doi.org/10.1155/2022/3567606

Research Article

Evaluation of 3,5-Diphenyl-2-Pyrazolines for Antimitotic Activity by Inhibition of Tubulin Polymerization

Soon Young Shin,[1] **Euitaek Jung**,[1] **Young Han Lee**,[1] **Yoongho Lim**,[2] **Seunghyun Ahn**,[3] **and Dongsoo Koh**[3]

[1]*Department of Biological Sciences, College of Biological Science and Biotechnology, Konkuk University, Seoul 05029, Republic of Korea*
[2]*Division of Bioscience and Biotechnology, BMIC, Konkuk University, Seoul 05029, Republic of Korea*
[3]*Department of Applied Chemistry, Dongduk Women's University, Seoul 02748, Republic of Korea*

Correspondence should be addressed to Dongsoo Koh; dskoh@dongduk.ac.kr

Received 8 July 2022; Revised 25 August 2022; Accepted 13 September 2022; Published 26 September 2022

Academic Editor: Wagdy Eldehna

Chalcones have a skeleton of diphenyls connected *via* an *α*,*β*-unsaturated carbonyl group. Many chalcone derivatives have been shown to interact with tubulin. Based on previous reports, chalcones derived by substitution of a carbonyl group with 2-pyrazoline can be expected to inhibit tubulin polymerization. Therefore, 3,5-diphenyl-2-pyrazolines were prepared to investigate their ability to inhibit tubulin polymerization. The clonogenic long-term survival assay showed that derivative **4**, 5-(3,5-dimethoxyphenyl)-3-(2-methoxyphenyl)-4,5-dihydro-1H-pyrazole-1-carbothioamide, was the most effective at inhibiting the clonogenicity of HCT116 human colon cancer cells. Derivative **4** induced G2/M cell cycle arrest. In addition, derivative **4** caused dispersed microtubules, a disorganized spherical arrangement of chromosomes, and inhibition of mitotic spindle formation. The binding mode between tubulin and derivative **4** was elucidated by *in silico* molecular docking. Derivative **4** was superimposed with colchicine and entered the colchicine-binding site well. These results suggest that derivative **4** inhibits tubulin polymerization by binding to the colchicine binding site of tubulin, thus preventing mitotic spindle formation during mitosis in HCT116 colon cancer cells. We propose that derivative **4** could be used as a promising antimitotic chemotherapeutic agent.

1. Introduction

The clinical usefulness of chemotherapeutic drugs is based on the differential effect of the drugs on normal versus cancerous cells. One of the various targets of chemotherapy is alteration of microtubule dynamics. Molecules that bind to tubulin to alter its incorporation into microtubules can be used as chemotherapeutic agents [1]. Tubulin *α*,*β* heterodimers interact with ligands at different sites, such as colchicine, vinca domain, maytansine, and pironectin sites [2].

Colchicine was the first microtubule-destabilizing molecule to be discovered and it inhibits mitosis. As cancer cells generally proliferate at a much faster rate than normal cells, colchicine has been investigated as a potential chemotherapeutic agent, although it has not been used as such [3]. Although colchicine is not used as an anticancer drug because of its low efficacy and high toxicity, including anemia and bone marrow damage, there have been extensive efforts to identify molecules that interact with the colchicine binding site. Although a chemotherapeutic agent that targets the colchicine binding site has yet to be developed, it is nonetheless still considered a potential target for anticancer drug development. Combretastatin isolated from *Combretum caffrum* have been shown to inhibit tubulin polymerization by interaction with the colchicine binding site [4]. These compounds are natural polyphenols that contain multiple phenol groups. Among these, chalcones have skeletons of diphenyls connected *via* an *α*,*β*-unsaturated carbonyl group, as shown in Figure S1. Many chalcone derivatives interact with tubulin. Chloro-substituted-2′-

hydroxychalcones have been studied as inhibitors of tubulin polymerization and cell proliferation [5]. As a natural chalcone with benzopyran, millepachine, exhibits anticancer activities, a derivative with a 4-diethylamino group as a substituent on the B ring was synthesized and shown to suppress tubulin polymerization in HepG2 cells and it was able to arrest HepG2 cells in G2/M phase [6].

Colorectal cancer is one of the most common cancers in both men and women worldwide and the second leading cause of cancer-related death in the United States [7]. HCT116 is a human colon carcinoma cell line that is commonly used in cancer biology research due to its characteristics, including aggressive oncogenic, invasive, undifferentiated, and growth factor-independent property. The authors designed and synthesized 2-hydroxy-2′,4′,6′-trimethoxy-5,6-benzochalcone, and they showed that it could disrupt the microtubule cytoskeleton of human colon cancer cells [8]. Another methoxylated benzochalcone synthesized by the authors, 2-hydroxy-4-methoxy-2′,3′-benzochalcone inhibited tubulin polymerization [9]. Naphthalene-chalcone derivatives interact with tubulin and lead to G_2/M cell cycle arrest and apoptosis [10, 11]. 3-(Naphthalen-2-yl)-N,5-diphenyl-pyrazoline-1-carbothioamide, prepared by substitution of the *α*,*β*-unsaturated carbonyl group of chalcone with 2-pyrazoline, has been shown to induce apoptosis and trigger cell death via a caspase-dependent mechanism [12].

Based on the previous results, chalcones derived by substitution of a carbonyl group with 2-pyrazoline can be expected to inhibit tubulin polymerization. Based on the pharmacophoric characteristics of colchicine, as shown in Figure 1, derivatives containing similar characteristics such as hydrogen bond acceptor, donor, and hydrophobic centers could be designed as colchicine-binding site inhibitors [13, 14]. 2,3′,5′-trimethoxy groups of 3,5-diphenyl-2-pyrazoline moiety contained in 19 derivatives satisfy hydrogen bond acceptor of the pharmacophoric characteristics shown in Figure 1. Benzene ring attached to thiazole (derivatives **6**–**12**) and benzylidene group attached to thiazolone (derivatives **13**–**19**) satisfy hydrophobic center of the pharmacophoric characteristics. Eighteen derivatives including 3,5-diphenyl-2-pyrazoline moiety (Figure S2) and a chalcone derivative, whose oxygen in the *α*,*β*-unsaturated carbonyl group was substituted with hydrazine were prepared and their inhibitory effects on tubulin polymerization were investigated. As mentioned above, disruption of microtubule dynamics is a property relevant to chemotherapeutic activity, the cytotoxicities of 3,5-diphenyl-2-pyrazoline derivatives toward cancer cells were determined using a clonogenic long-term survival assay. Among the 3,5-diphenyl-2-pyrazoline derivatives, derivative **4**, 5-(3,5-dimethoxyphenyl)-3-(2-methoxyphenyl)-4,5-dihydro-1H-pyrazole-1-carbothioamide, exhibited the greatest half-maximal cell growth inhibitory effect. It inhibited tubulin polymerization, similar to colchicine, and arrested the cell cycle in G_2/M phase. The molecular binding mode between tubulin and derivative **4** was elucidated by *in silico* docking, which demonstrated that it fits the colchicine binding site well.

2. Materials and Methods

2.1. Design and Synthesis of Derivatives. Eighteen 3,5-diphenyl-2-pyrazoline derivatives and a chalcone derivative, whose oxygen in the *α*,*β*-unsaturated carbonyl group was substituted with hydrazine, were synthesized, and their spectroscopic data obtained from NMR spectroscopy and mass spectrometry were previously reported by the authors [15]. In the current research, their activities against HCT116 human colon cancer cells were investigated. Their chemical structures are shown in Figure 2.

2.2. Cell Culture. Human colon cancer cells (HCT116) were obtained from the American Type Culture Collection (Rockville, MD, USA). The cells were cultured in Dulbecco's Modified Eagle's Medium (DMEM) supplemented with 10% (v/v) heat-inactivated fetal bovine serum (HyClone, Logan, UT, USA).

2.3. Clonogenic Long-Term Survival Assay. Clonogenic assays were performed as previously described [16] with a minor modification. In brief, HCT116 cells (4×10^3 cells per well) were treated with different concentrations of the compounds (0, 1, 5, 10, and 20 μM) for 7 days, followed by fixation with 6% glutaraldehyde and staining with 0.1% crystal violet.

2.4. Cell Cycle Analysis. The cell cycle was analyzed by flow cytometry as previously described [17]. In brief, HCT116 cells were treated with 100 ng/mL colchicine or 40 μM derivative **4** for 24 h, fixed in 70% ethanol, and stained with propidium iodide (50 μg/mL) in RNase buffer (50 μg/mL RNase A, 0.1% Triton X-100, and 0.1 mM EDTA). 'The cells were classified as G1, S, or G2/M phase depending on the diploid to tetraploid DNA contents. The percentage of the cell population in each cell cycle phase was determined using a NucleoCounter® NC-3000™ cytometer (ChemoMetec, Allerød, Denmark).

2.5. In silico Docking. Among the many 3D structures of tubulin deposited in the protein data bank, the 6xer.pdb was selected because it contains colchicine as its ligand [18]. *In silico* docking was performed using AutoDock Vina (The Scripps Research Institute, La Jolla, USA) as described previously [19]. The holoprotein was prepared using the UCSF Chimera visualization system [20]. The structure of derivative **4** was modified based on the 3D structure of 3,5-diphenyl-2-pyrazoline deposited in PubChem (PubChem CID 3683844) using the Sybyl 7.3/Sketch module. The modified derivative **4** was subjected to energy minimization using the molecular mechanics algorithms provided by Sybyl 7.3. Minimization ceased when the total energy was converged to 0.05 kcal/molÅ. Systematic conformational searches were performed using Sybyl 7.3/Molecular Dynamics module and the conformer with the lowest energy was selected as the three-dimensional (3D) structure of derivative 4 [21, 22]. To validate the docking process, the molecular dynamics (MD) simulation was performed using Sybyl 7.3/molecular dynamics module.

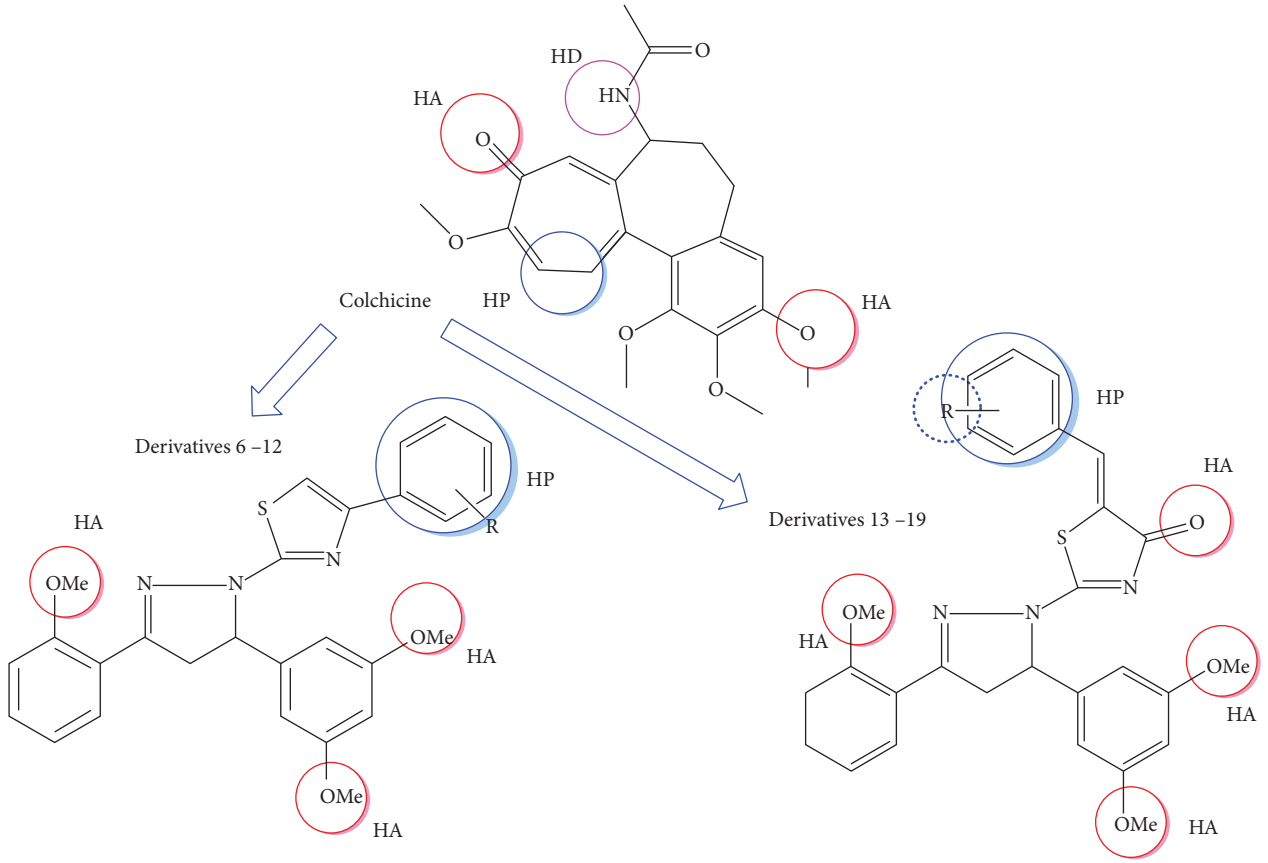

Figure 1: Schematic representation of the pharmacophoric characteristics of the derivatives where HA, HD, and HP denote hydrogen bond acceptor, donor, and hydrophobic centers, respectively.

2.6. Immunofluorescence Microscopy. HCT116 cells cultured on coverslips were treated with either vehicle (dimethyl sulfoxide) or 40 μM derivative **4**. After 24 h, the cells were fixed with 4% paraformaldehyde and permeabilized using 0.1% Triton X-100, as previously described [23]. The cells were then incubated with mouse anti-α,β-tubulin (1 : 500 dilution, Invitrogen) and rabbit antipericentrin (1 : 500 dilution, Invitrogen) antibodies for 2 h. After rinsing, the slides were double-labeled with red-fluorescent ALexa Fluor® 555-conjugated antimouse and green-fluorescent Alexa Fluor 488®-conjugated antirabbit antibodies (Invitrogen, Carlsbad, CA, USA) for 30 min. The nuclear DNA was stained with Hoechst 33258 (Sigma-Aldrich). Cells were imaged using an EVOSf1 fluorescence microscope (Advanced Microscopy Group, Bothell, WA, USA).

3. Results and Discussion

3.1. The Effect of 3,5-Diphenyl-2-Pyrazoline Derivatives on Clonogenicity of HCT116 Cells. To confirm whether 3,5-diphenyl-2-pyrazoline derivatives exhibit anticancer activities, their ability to inhibit the proliferation of cancer cell lines was evaluated using a clonogenic long-term survival assay. The inhibitory effects on the colony growth of HCT116 human colon cancer cells at different concentrations (0, 1, 5, 10, and 20 μM) of the derivatives were determined, as shown in Figure 3(a). Some derivatives, including **4**, **6**, **9**, **10**, **11**, and **12** were tested at low concentrations (0, 0.1, 0.5, 1, and 5 μM) because they exhibited potent inhibitory effects (Figure 3(b)). The half-maximal cancer cell growth inhibitory concentrations (GI_{50}) were determined using densitometry and SigmaPlot software (SYSTAT, Chicago, IL, USA), as previously described [22]. The GI_{50} values of the 3,5-diphenyl-2-pyrazoline derivatives are listed in Table 1, and the error bars are shown in Figure S3. The GI_{50} values ranged between 0.09 and 14.82 μM. These data suggest that 3,5-diphenyl-2-pyrazoline derivatives differentially inhibited the growth of HCT116 colon cancer cells. The half-maximal cell growth inhibitory activities caused by substituents at 1-*N* of 5-(3,5-dimethoxyphenyl)-3-(2-methoxyphenyl)-4,5-dihydro-1*H*-pyrazole increase as follows: thiazol-4(5*H*)-one (derivative **5**) < methanethial (derivative **2**) < acetaldehyde (derivative **3**) < methanethioamide (derivative **4**). In the case of 2-(5-(3,5-dimethoxyphenyl)-3-(2-methoxyphenyl)-4,5-dihydro-1*H*-pyrazol-1-yl)-4-phenylthiazole moiety, the activities decrease as follows: *m*-F (derivative **10**) > *p*-OMe (derivative **7**) > *m*-OMe (derivative **6**) > *p*-Cl (derivative **12**) > *p*-F (derivative **11**) > *o*-F (derivative **9**) > *p*-CN (derivative **8**). In (*Z*)-5-benzylidene-2-(5-(3,5-dimethoxyphenyl)-3-(2-methoxyphenyl)-4,5-dihydro-1*H*-pyrazol-1-yl)thiazol-4(5*H*)-one moiety, the activities decrease as follows: *o*-OMe (derivative **13**) > *o,m*-di-OMe (derivative **16**) > *m*-OMe (derivative **14**) > *p*-OMe (derivative **15**) > *m,m*-di-OMe

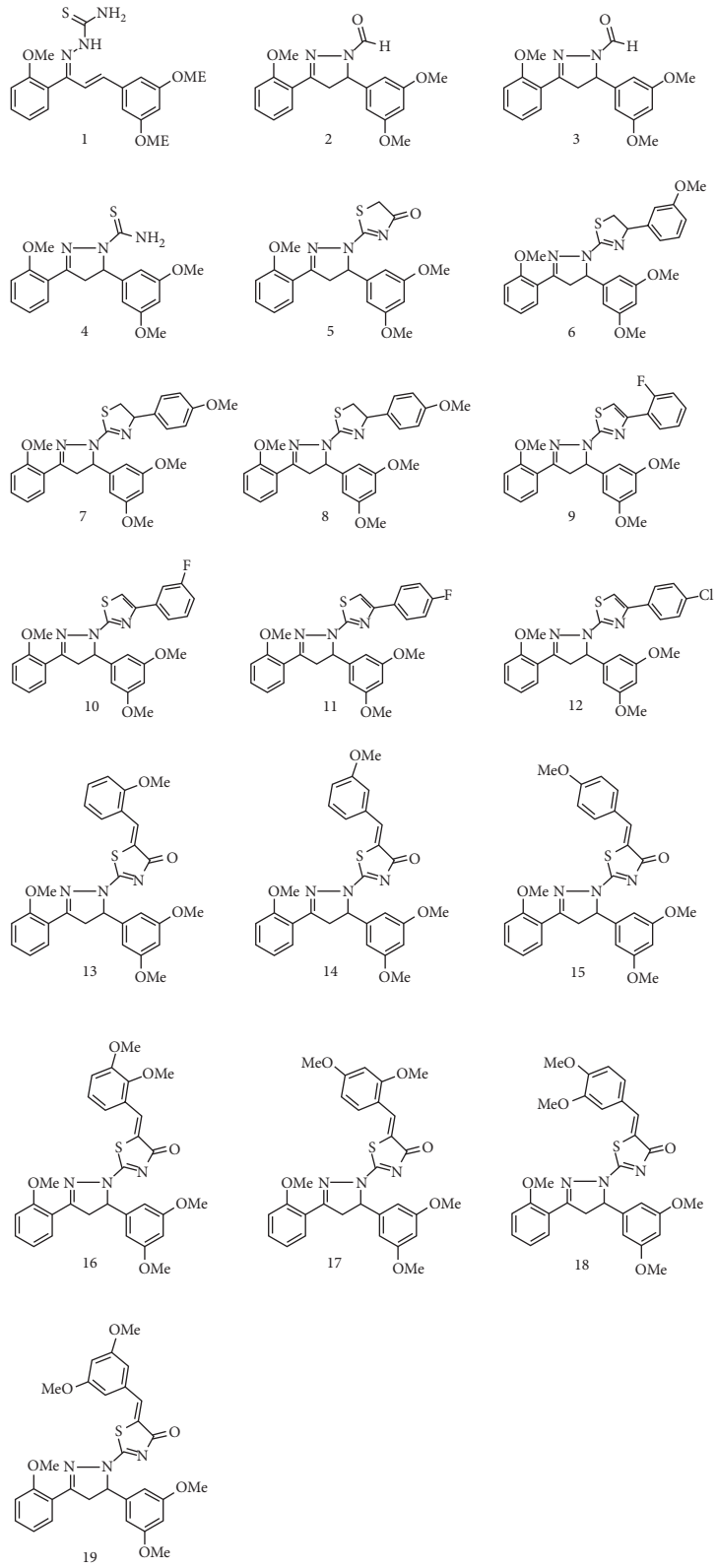

Figure 2: The chemical structures of 3,5-diphenyl-2-pyrazoline derivatives.

(derivative **19**) > *o,p*-di-OMe (derivative **17**) = *m,p*-di-OMe (derivative **18**). Structures of the 3,5-diphenyl-2-pyrazoline derivatives and their GI50 structure-activity relationships (SARs) are shown in Figure 4. While derivative **1** consists of an open bridge between diphenyl rings, two phenyl rings of 18 derivatives are connected via 2-pyrazoline. As described in the introduction section, we focused on the activities of 3,5-diphenyl-2-pyrazoline

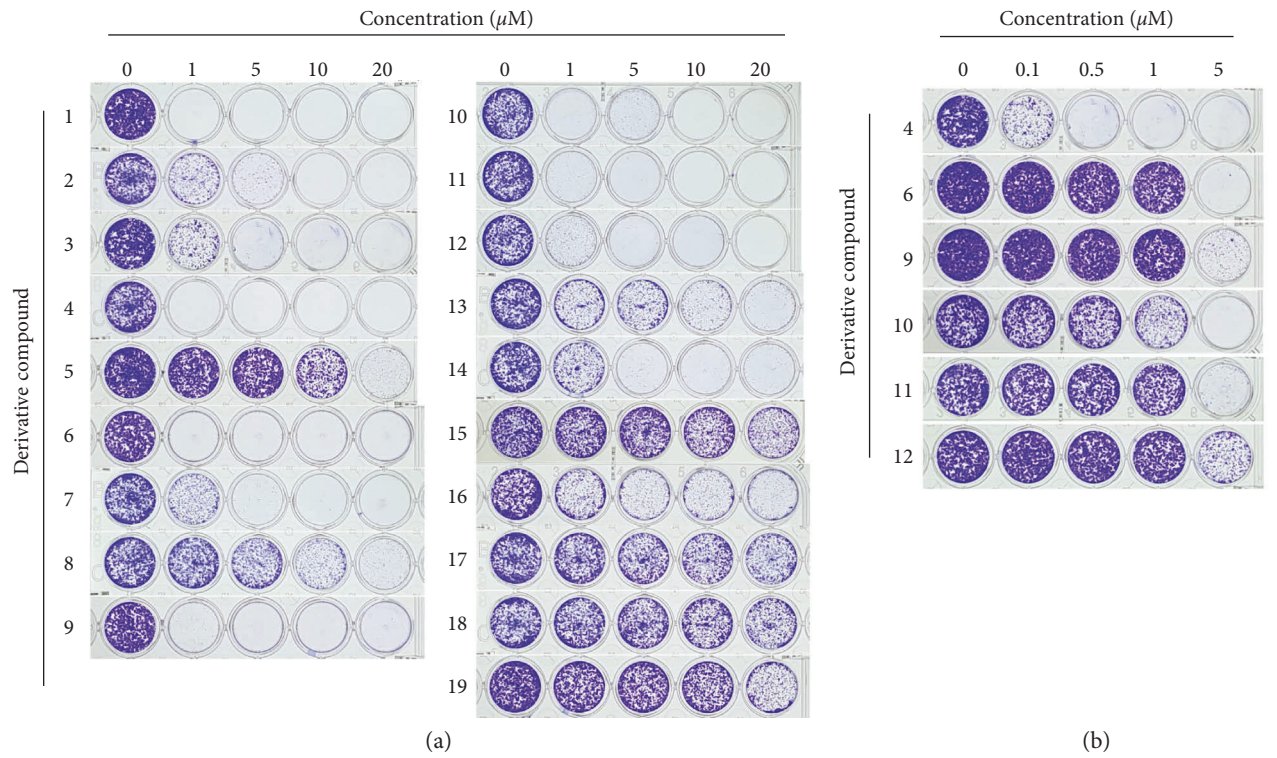

Figure 3: (a) Clonogenic long-term survival assay of 3,5-diphenyl-2-pyrazoline derivatives against HCT116 human colon cancer cells at different concentrations (0, 1, 5, 10, and 20 μM) and (b) of derivatives **4**, **6**, **9**, **10**, **11**, and **12** at lower concentrations (0, 0.1, 0.5, 1, and 5 μM).

Table 1: The half-maximal cell growth inhibitory concentrations (GI_{50}) of 3,5-diphenyl-2-pyrazolines obtained by the clonogenic long-term survival assay of HCT116 human colon cancer cells.

Derivatives	$GI_{50}/\mu M$	Standard deviation
1	0.09	0.00
2	0.94	0.00
3	0.93	0.00
4	0.09	0.00
5	9.74	0.06
6	1.47	0.03
7	0.97	0.00
8	6.07	0.12
9	2.11	0.04
10	0.80	0.00
11	2.01	0.06
12	1.84	0.01
13	0.95	0.00
14	0.98	0.00
15	11.94	0.24
16	0.98	0.00
17	Not detected	—
18	Not detected	—
19	14.82	0.23

derivatives. Therefore, we selected derivative **4** for further biological study even though derivatives **1** and **4** showed similar activities in the inhibition of clonogenicity of cancer cells.

3.2. The Effect of Derivative 4 on Cell Cycle Progression. To investigate the mechanism of action of the colony growth inhibition of HCT116 cancer cells by 3,5-diphenyl-2-pyrazoline derivatives, we tested the effect of derivative **4**, which exhibited the best GI_{50} value, on cell cycle progression. HCT116 cells were treated with 40 μM derivative **4** for 24 h, and changes in the distribution of the number of cells in the various cell cycle phases were examined by flow cytometry. As a reference compound, 100 ng/mL colchicine was used. Notably, derivative **4** treatment increased the cell population in the G_2/M phase from 25% to 63% after 24 h, with a concomitant decrease in the number of cells in the G_0/G_1 phase (Figure 5(a)). In addition, the percentage of sub-G_0/G_1 cells, representing apoptotic cells, increased slowly, but steadily, after exposure to derivative **4**. Cyclins are a family of proteins that control cell cycle progression by activating cyclin-dependent kinases (CDKs) at different stages of the cell cycle. Upon the addition of derivative **4**, cyclin E and cyclin A levels progressively decreased over 24 h after treatment (Figure 5(b)). In contrast, cyclin B1 levels increased by 12 h and declined at 24 h. As cyclin B levels begin to increase before entering mitosis and decline during metaphase and anaphase as cells reenter the next G1 phase [24], we suggest that derivative **4** triggers the cell cycle arrest at the G2/M phase, resulting in the growth of HCT116 cells.

3.3. The Effect of Derivative 4 on the Mitotic Spindle Network. Inhibition of microtubule dynamics leads to disruption of the mitotic spindle in dividing cells and hence results in M phase cell cycle arrest [25]. We used antitubulin immunofluorescence microscopy to examine the effect of derivative **4** on the arrangement of the microtubule cytoskeleton. Vehicle-treated mitotic cells had mitotic spindles that were

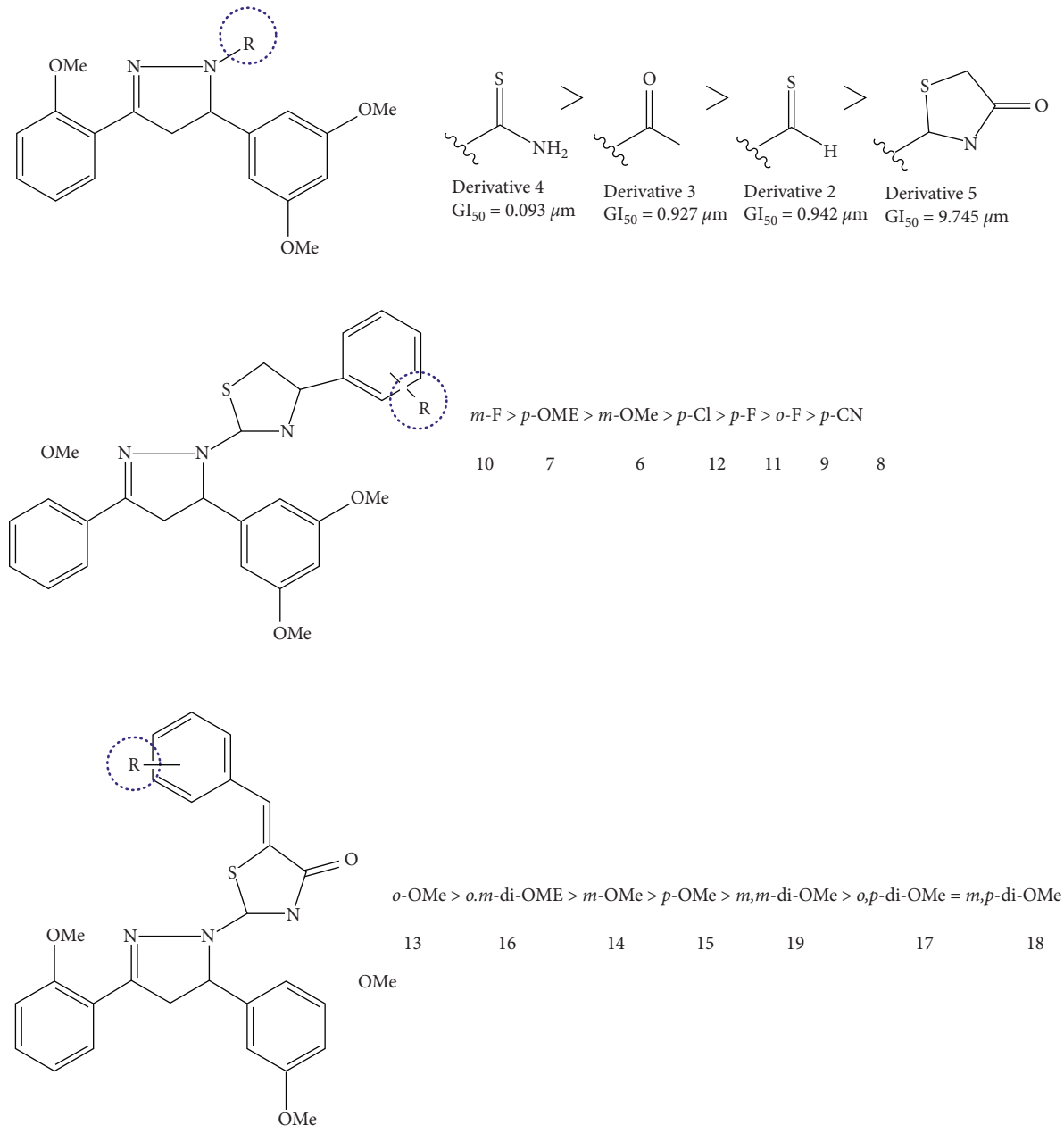

Figure 4: Structures of the 3,5-diphenyl-2-pyrazoline derivatives and their GI_{50} structure-activity relationships (SARs).

attached to chromosomes aligned at the metaphase equatorial plate. However, in the presence of derivative **4,** the mitotic cells exhibited densely dispersed microtubules and a disorganized spherical arrangement of chromosomes (Figure 6, top panel). The centrosome, composed of a pair of centrioles, is a cellular organelle that controls the cell cycle and regulates mitotic spindle formation and chromosome segregation [26]. At the G_2/M transition, the duplicated centrosomes separate and move to opposite poles of the cell by a process known as centrosome maturation. Pericentrin is a centrosome component involved in microtubule organization [27]. To address whether derivative **4** caused abnormal mitotic spindle formation, we stained the cells for pericentrin. In vehicle-treated cells, pericentrin was typically located at the edge of the bipolar spindles attached to chromosomes. However, in the presence of derivative **4**, the distribution of pericentrin was abnormal, with singlet or doublet dots within spherically arranged chromosomes (Figure 6, third panel). These data suggest that derivative **4** inhibits mitotic spindle formation, leading to the incomplete microtubule networks during mitosis, which results in M phase cell cycle arrest.

3.4. Prediction of the α,β-Tubulin Binding Site of Derivative 4 through In Silico Docking Simulation. To gain insight into the mechanism by which derivative **4** inhibits mitotic spindle formation, we tested whether derivative **4** binds to tubulin *α,β*-dimer. The binding mode between tubulin and derivative **4** was elucidated by *in silico* molecular docking. Since

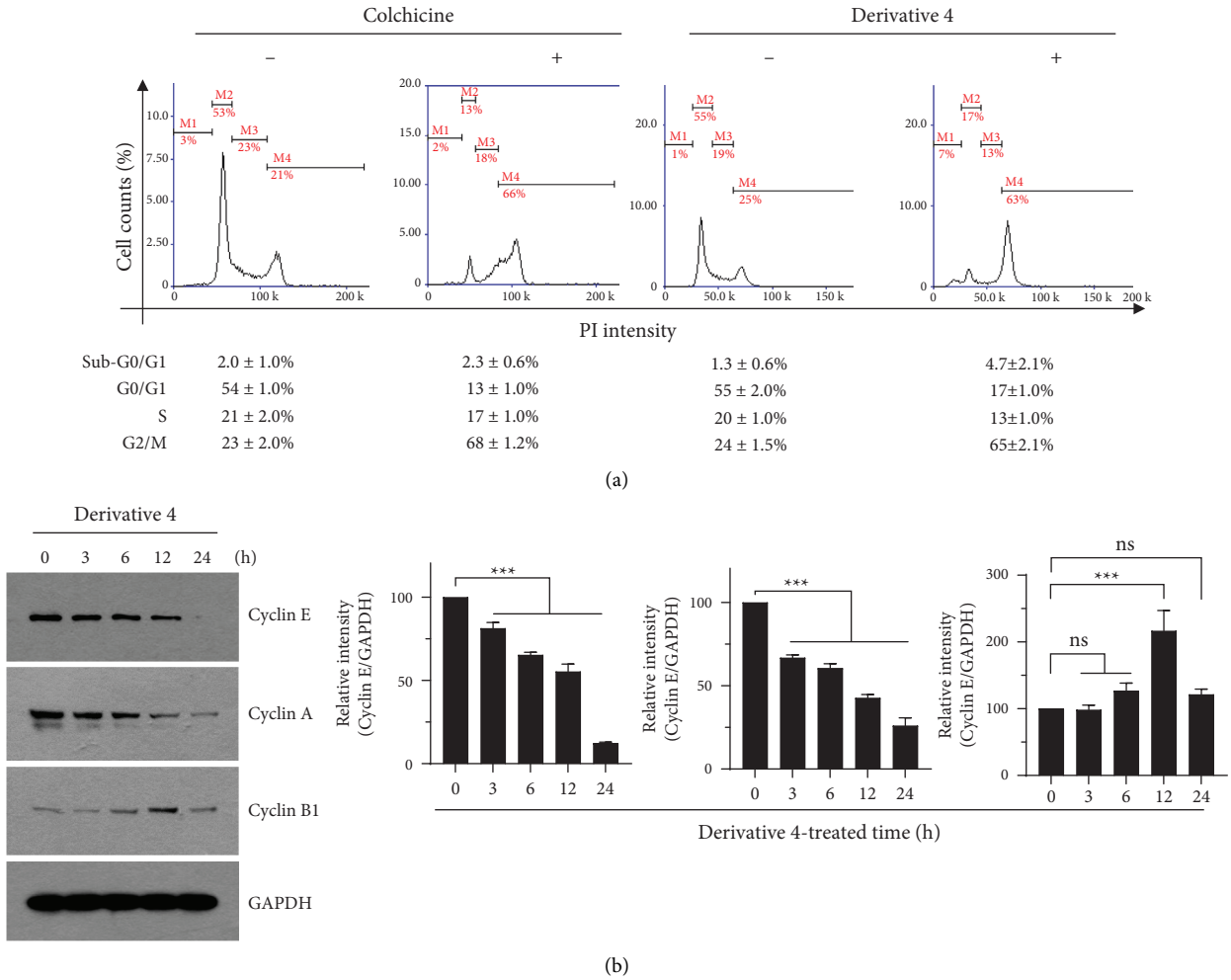

Figure 5: effect of derivative **4** on cell cycle progression. (a) HCT116 cells were either untreated or treated with 100 ng/mL colchicine or 40 μM derivative 4 for 24 h. The cellular DNA was stained with propidium iodide, and the DNA contents were determined by flow cytometry. M1, sub-G0/G1; M2, G0/G1; M3, S; and M4, G2/M. x-axis, DNA contents; y-axis, cell counts (%). Data represent mean ± S.D. ($n = 3$). (b) HCT116 cells were treated with 40 μM derivative **4** for different time periods. Total cell lysates were prepared and subjected to immunoblotting using antibodies against cyclin E cyclin A and cyclin B1. GAPDH was used as a loading control. For the quantification, the relative band intensity corresponding to each protein was normalized to the GAPDH level using ImageJ software. Data are expressed as mean ± S.D. ($n = 3$). ns, not significant; $^{***}P < 0.001$ ($n = 3$) by the Dunnett's multiple comparison test.

6xer.pdb contains colchicine as its ligand, its structure was used in *in silico* docking [18]. It consists of two α,β-tubulin heterodimers and stathmin-4. Since the colchicine site is located between the tubulin heterodimers, one α,β-tubulin heterodimer and stathmin-4 were deleted using the UCSF Chimera visualization system. To obtain the solution structure of the α, β-tubulin holo-protein without colchicine and stathmin-4 prepared by chimera, energy minimization was carried out using Sybyl 7.3/energy minimization module. This holoprotein was used in *in silico* docking. *In silico* docking experiments were performed using *AutoDock Vina* (The Scripps Research Institute, San Diego, CA, USA). The grid box was determined using AutoDock Tools (ADT; Scripps Research Institute). The grid box for the docking procedure was set as follows: the centers of x, y, and z were −7.639, −9.167, and 39.472, respectively, and the sizes of x, y, and z were 18, 20, and 18, respectively. To confirm whether the current docking procedure was correct, colchicine was docked into the α,β-tubulin holoprotein. The binding energy between the α,β-tubulin holoprotein and colchicine was −10.4 kcal/mol, and the binding pose was superimposed on the crystal structure 6xer.pdb well (Figure S4). Therefore, the docking procedure was considered to be effective. To validate the docking procedure, the MD simulation was carried out at the length of 100 nsec. The kinetic energy of colchicine was stable over the simulation time as shown in Figure S5A. Derivative **4** was docked into the α,β-tubulin holoprotein in the same manner, and its binding energy was −8.0~−6.4 kcal/mol. As shown in Figure 7, its binding pose was similar to that of colchicine. For the validation of the docking process for derivative **4**, the MD simulation was performed, and its kinetic energy was stable at 100 nsec, as shown in Figure S5B. The residues participating in the binding site of colchicine were compared with those of

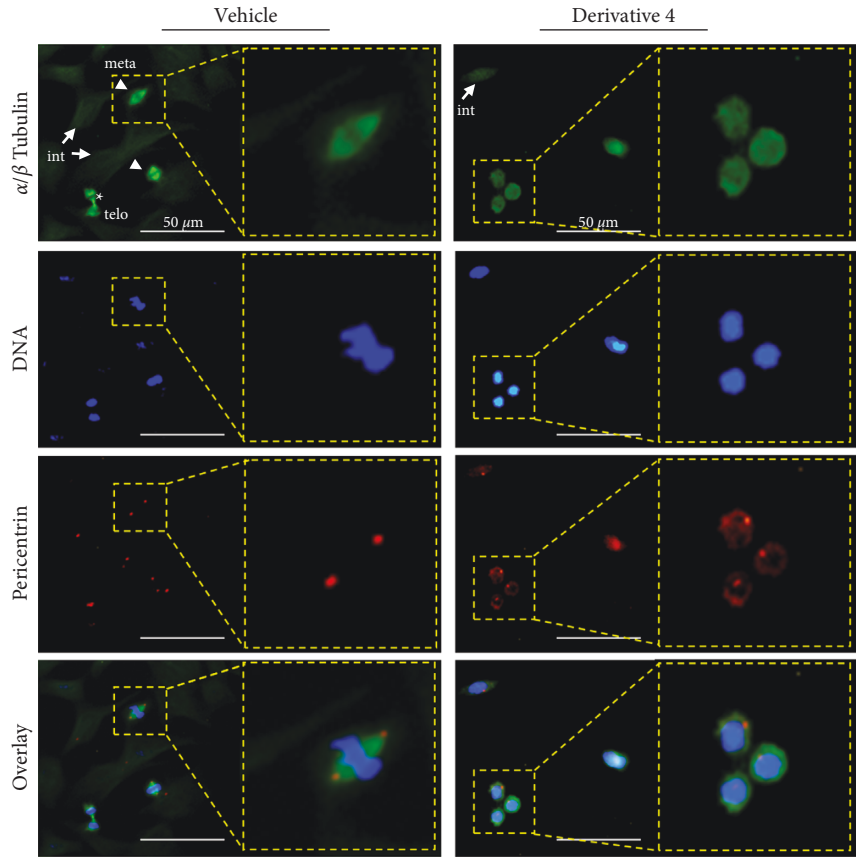

Figure 6: effect of derivative **4** on mitotic spindle formation. HCT116 cells cultured on coverslips were treated with 40 μM derivative **4** for 24 h The cells were fixed and incubated with antibodies against α,β-tubulin and pericentrin for 2 h followed by incubation with an AlexaFluor 488-conjugated (for α,β-tubulin, green signal) and AlexaFluor 555-conjugated (for pericentrin, red spot) secondary antibodies for 30 min. Nuclear DNA was stained with 1 μg/mL Hoechst 33258 for 10 min (blue signal). M phase cells were selected and analyzed for assembly of mitotic spindles. The fluorescent signals were imaged using an EVOSf1® fluorescence microscope. Arrows, interphase cells (int); arrowheads, metaphase spindle (meta); star-like, telophase spindle (telo). Scale bars, 50 μm.

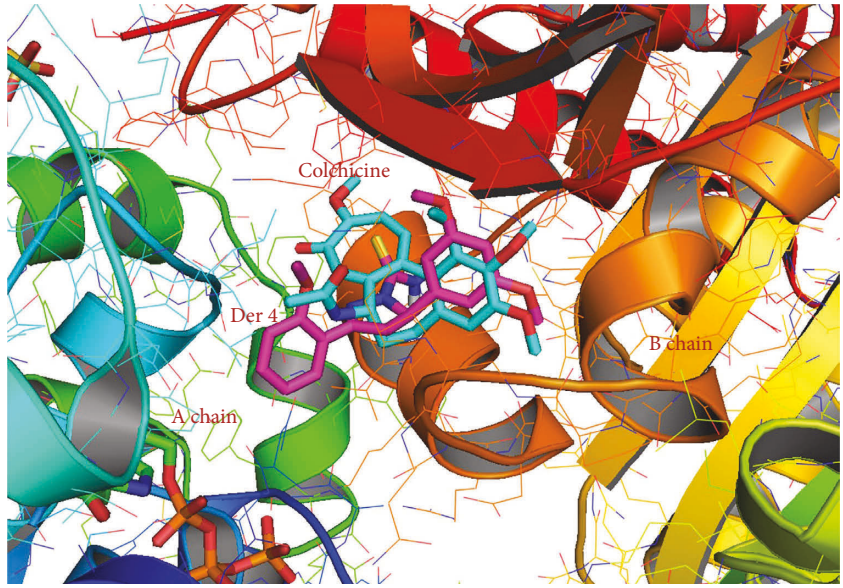

Figure 7: The 3D images of colchicine (cyan) and derivative **4** (magenta) contained in the binding pocket of 6xer.pdb generated using PyMol (the PyMOL Molecular Graphics System, Schrödinger, LLC).

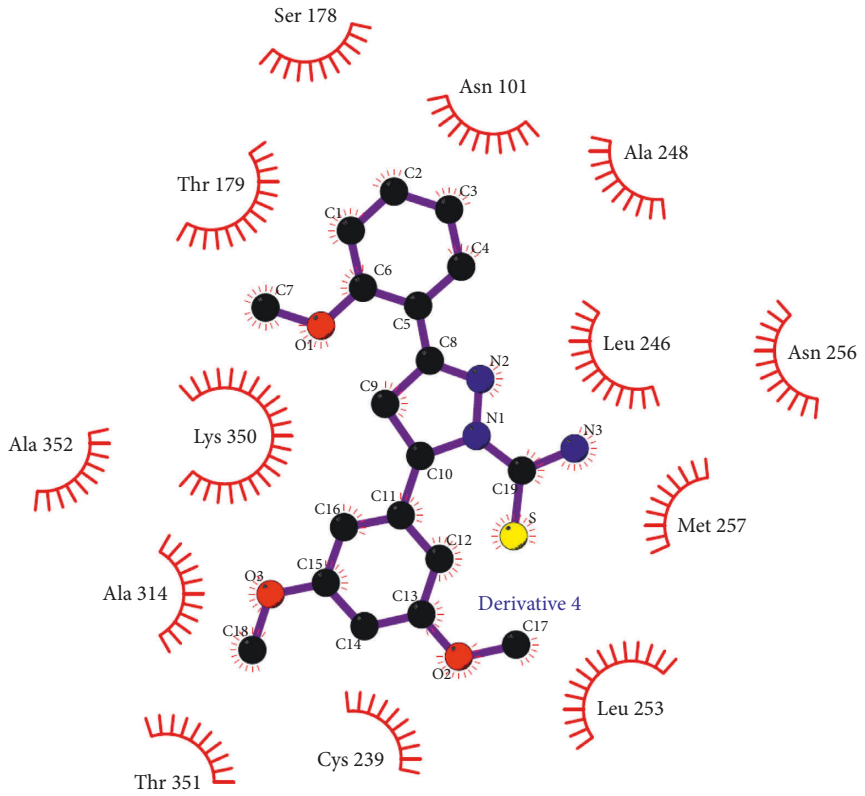

Figure 8: Interactions between derivative **4** and residues of the holoprotein of 6xer.pdb analyzed using LIGPLOT. All residues in the red half-circles denote hydrophobic interactions.

derivative **4** using the LigPlot program [28]. In the colchicine-α,β-tubulin holoprotein complex, hydrophobic interactions were formed by 19 residues, including S178(A), T179(A), A180(A), C239, L240, L246, A248, D249, K252, L253, N256, M257, T312, V313, A314, I316, N348, K350, and A352, and a hydrogen bond was observed between the nitrogen of V181(A) and the hydroxyl group of colchicine (2.88 Å), where (A) denotes residues of the A chain and the other residues belong to the B chain (Figure 1). In the derivative **4**, the α,β-tubulin holoprotein complex and hydrophobic interactionswere formed by 13 residues, including N101(A), S178(A), T179(A), C239, L246, A248, L253, N256, M257, A314, K350, T351, and A352 (Figure 8). Two residues, N101(A) and T351, were not detected for colchicine. As shown in Figure 7, the hydroxyl group of colchicine is close to V181, but derivative **4** is far away. As a result, there was no hydrogen bond to derivative **4**. It can be considered that a lesser number of residues participating in binding results in poor binding energy values. However, derivative **4** was superimposed with colchicine and readily entered the colchicine binding site.

Since there is a big problem in the solubility of the colchicine binding site inhibitors, the aqueous solubility of derivative **4** was assessed using SwissADME provided by the Swiss Institute of Bioinformatics (https://www.sib.swiss/). The lipophilicity of derivative **4** was determined based on iLogP of 3.44. Because the iLogP of colchicine is 3.28, derivative **4** is considered to show similar lipophilicity to colchicine. Water solubility was determined using the decimal logarithm of the molar solubility in water (logS). While the logS values of colchicine obtained by three models namely ESOL, Ali, and SILICOS-IT were 0.502, 1.72, and 8.76×10^{-5} mg/mL, respectively, those of derivative **4**, 6.58×10^{-2}, 1.41×10^{-2}, and 3.67×10^{-3} mg/mL, respectively. This result demonstrated derivative **4** is moderately water soluble [29].

4. Conclusion

The GI_{50} values showing the half-maximal cell growth inhibitory effects against HCT116 human colon cancer cells caused by nineteen 3,5-diphenyl-2-pyrazoline derivatives ranged between 0.09 and 14.82 μM. Because 5-(3,5-dimethoxyphenyl)-3-(2-methoxyphenyl)-4,5-dihydro-1*H*-pyrazole-1-carbothioamide (derivative **4**) showed the best effect (90 nM), further biological experiments were carried out using derivative **4** to investigate the mechanism of action by 3,5-diphenyl-2-pyrazoline derivatives. Derivative **4** inhibited tubulin polymerization by binding to the colchicine binding site on tubulin, thus disrupting mitotic spindle formation during mitosis in HCT116 colon cancer cells. As proper assembly of the mitotic spindle microtubules is essential for the segregation of chromosomes to the two daughter cells during cell division, derivative **4** was tested whether it binds two tubulin α,β-dimer through *in silico* docking simulation. Even the interactions between the residues surrounding the colchicine binding site of tubulin and derivative **4** were

slightly different with those of colchicine, the 3D image showing the docking pose of derivative **4** was superimposed with that of colchicine and it readily entered the colchicine binding site. As a result, we propose that derivative **4** could be a promising antimitotic chemotherapeutic agent.

Data Availability

The datasets used and analyzed to support this study are available from the corresponding author upon request.

Conflicts of Interest

The authors declare that there are no conflicts of interest regarding the publication of this paper.

Acknowledgments

The authors acknowledge financial support from the Basic Science Research Program (award no. NRF-2021R1F1A1052699). S.Y. Shin was supported by the KU Research Professor Program of Konkuk University.

Supplementary Materials

Figure S1: the chemical structure and numbering of chalcone. Figure S2: the chemical structure of 3,5-diphenyl-2-pyrazoline. Figure S3: graph of the half-maximal cell growth inhibitory concentrations (GI50) of 3,5-diphenyl-2-pyrazoline derivatives (with error bars). Figure S4: 3D images of colchicine obtained from the current docking (pink) and colchicine contained in the crystallographic structure of tubulin 6xer.pdb as its ligand (cyan) in the binding pocket of the 6xer.pdb generated using PyMol. Figure S5: plots of kinetic energy of the colchicine-tubulin complex (A) and derivative **4** (B) against the simulation time 100 nsec. Figure S6: interactions between colchicine and residues of the holoprotein of 6xer.pdb analyzed using LigPlot. Residues in the red half-circles denote hydrophobic interactions, and Val181 of the A chain forms a hydrogen bond with colchicine. Figure S7: 3D images of colchicine (cyan) and derivative **4** (magenta) contained in the binding pocket of 6xer.pdb generated using PyMol. The hydroxyl group of colchicine forms a hydrogen bond with the nitrogen of Val181 of the A chain (2.9 Å). (*Supplementary Materials*)

References

[1] Y. Lu, J. Chen, M. Xiao, W. Li, and D. D. Miller, "An overview of tubulin inhibitors that interact with the colchicine binding site," *Pharmaceutical Research*, vol. 29, no. 11, pp. 2943–2971, 2012.

[2] D. Alpízar-Pedraza, A. d. l. N. Veulens, E. C. Araujo, J. Piloto-Ferrer, and Á. Sánchez-Lamar, "Microtubules destabilizing agents binding sites in tubulin," *Journal of Molecular Structure*, vol. 1259, Article ID 132723, 2022.

[3] F. Naaz, M. R. Haider, S. Shafi, and M. S. Yar, "Anti-tubulin agents of natural origin: targeting taxol, vinca, and colchicine binding domains," *European Journal of Medicinal Chemistry*, vol. 171, pp. 310–331, 2019.

[4] S. N. A. Bukhari, G. B. Kumar, H. M. Revankar, and H. L. Qin, "Development of combretastatins as potent tubulin polymerization inhibitors," *Bioorganic Chemistry*, vol. 72, pp. 130–147, 2017.

[5] H. Aryapour, G. H. Riazi, A. Foroumadi et al., "Biological evaluation of synthetic analogues of curcumin: chloro-substituted-2′-hydroxychalcones as potential inhibitors of tubulin polymerization and cell proliferation," *Medicinal Chemistry Research*, vol. 20, no. 4, pp. 503–510, 2011.

[6] G. Wang, W. Wu, F. Peng et al., "Design, synthesis, and structure–activity relationship studies of novel millepachine derivatives as potent antiproliferative agents," *European Journal of Medicinal Chemistry*, vol. 54, pp. 793–803, 2012.

[7] A. Bhandari, M. Woodhouse, and S. Gupta, "Colorectal cancer is a leading cause of cancer incidence and mortality among adults younger than 50 years in the USA: a SEER-based analysis with comparison to other young-onset cancers," *Journal of Investigative Medicine*, vol. 65, no. 2, pp. 311–315, 2017.

[8] J. M. Lee, M. S. Lee, D. Koh, Y. H. Lee, Y. Lim, and S. Y. Shin, "A new synthetic 2′-hydroxy-2, 4, 6-trimethoxy-5′, 6′-naphthochalcone induces G2/M cell cycle arrest and apoptosis by disrupting the microtubular network of human colon cancer cells," *Cancer Letters*, vol. 354, no. 2, pp. 348–354, 2014.

[9] S. Y. Shin, J. H. Kim, H. Yoon et al., "Novel antimitotic activity of 2-hydroxy-4-methoxy-2′, 3′-benzochalcone (HymnPro) through the inhibition of tubulin polymerization," *Journal of Agricultural and Food Chemistry*, vol. 61, no. 51, pp. 12588–12597, 2013.

[10] G. Wang, W. Liu, Z. Gong, Y. Huang, Y. Li, and Z. Peng, "Synthesis, biological evaluation, and molecular modelling of new naphthalene-chalcone derivatives as potential anticancer agents on MCF-7 breast cancer cells by targeting tubulin colchicine binding site," *Journal of Enzyme Inhibition and Medicinal Chemistry*, vol. 35, no. 1, pp. 139–144, 2020.

[11] G. Wang, Z. Peng, J. Zhang, J. Qiu, Z. Xie, and Z. Gong, "Synthesis, biological evaluation and molecular docking studies of aminochalcone derivatives as potential anticancer agents by targeting tubulin colchicine binding site," *Bioorganic Chemistry*, vol. 78, pp. 332–340, 2018.

[12] Y. Lee, B. S. Kim, S. Ahn et al., "Anticancer and structure-activity relationship evaluation of 3-(naphthalen-2-yl)-N, 5-diphenyl-pyrazoline-1-carbothioamide analogs of chalcone," *Bioorganic Chemistry*, vol. 68, pp. 166–176, 2016.

[13] M. M. Hammouda, A. A. Elmaaty, M. S. Nafie et al., "Design and synthesis of novel benzoazoninone derivatives as potential CBSIs and apoptotic inducers: *in Vitro, in Vivo*, molecular docking, molecular dynamics, and SAR studies," *Bioorganic Chemistry*, vol. 127, Article ID 105995, 2022.

[14] I. H. Eissa, M. A. Dahab, M. K. Ibrahim et al., "Design and discovery of new antiproliferative 1, 2, 4-triazin-3(2H)-ones as tubulin polymerization inhibitors targeting colchicine binding site," *Bioorganic Chemistry*, vol. 112, Article ID 104965, 2021.

[15] B. Kim, S. Ahn, Y. Lee, D. Koh, and Y. Lim, "(1) H and (13) C NMR spectral assignments of nineteen 5-(3, 5-dimethoxyphenyl)-3-(2-methoxyphenyl)-2-pyrazoline derivatives," *Magnetic Resonance in Chemistry*, vol. 59, no. 4, pp. 478–488, 2021.

[16] N. A. P. Franken, H. M. Rodermond, J. Stap, J. Haveman, and C. van Bree, "Clonogenic assay of cells in vitro," *Nature Protocols*, vol. 1, no. 5, pp. 2315–2319, 2006.

[17] E. Jung, D. Koh, Y. Lim, S. Y. Shin, and Y. H. Lee, "Overcoming multidrug resistance by activating unfolded protein response of the endoplasmic reticulum in cisplatin-resistant A2780/CisR ovarian cancer cells," *BMB Reports*, vol. 53, no. 2, pp. 88–93, 2020.

[18] H. Chen, S. Deng, N. Albadari et al., "Design, synthesis, and biological evaluation of stable colchicine-binding site tubulin inhibitors 6-Aryl-2-benzoyl-pyridines as potential anticancer agents," *Journal of Medicinal Chemistry*, vol. 64, no. 16, pp. 12049–12074, 2021.

[19] O. Trott and A. J. Olson, "AutoDock Vina: improving the speed and accuracy of docking with a new scoring function, efficient optimization, and multithreading," *Journal of Computational Chemistry*, vol. 31, no. 2, pp. 455–461, 2010.

[20] E. F. Pettersen, T. D. Goddard, C. C. Huang et al., "UCSF Chimera—a visualization system for exploratory research and analysis," *Journal of Computational Chemistry*, vol. 25, no. 13, pp. 1605–1612, 2004.

[21] S. Y. Shin, H. Yoon, S. Ahn et al., "Chromenylchalcones showing cytotoxicity on human colon cancer cell lines and in silico docking with aurora kinases," *Bioorganic & Medicinal Chemistry*, vol. 21, no. 14, pp. 4250–4258, 2013.

[22] B. S. Kim, S. Y. Shin, S. Ahn, D. Koh, Y. H. Lee, and Y. Lim, "Biological evaluation of 2-pyrazolinyl-1-carbothioamide derivatives against HCT116 human colorectal cancer cell lines and elucidation on QSAR and molecular binding modes," *Bioorganic & Medicinal Chemistry*, vol. 25, no. 20, pp. 5423–5432, 2017.

[23] M. S. Lee, Y. Yong, J. M. Lee, D. Koh, S. Y. Shin, and Y. H. Lee, "A novel methoxyflavonol derivative, 2-hydroxy-3-(2-methoxyphenyl)-1H-Benzo[f]chromen-1-one (DK98), induces apoptosis in HCT116 human colon cancer cells," *Journal of the Korean Society for Applied Biological Chemistry*, vol. 57, no. 1, pp. 129–132, 2014.

[24] H. K. Matthews, C. Bertoli, and R. A. M. de Bruin, "Cell cycle control in cancer," *Nature Reviews Molecular Cell Biology*, vol. 23, no. 1, pp. 74–88, 2022.

[25] F. Mollinedo and C. Gajate, "Microtubules, microtubule-interfering agents and apoptosis," *Apoptosis*, vol. 8, no. 5, pp. 413–450, 2003.

[26] S. Doxsey, W. Zimmerman, and K. Mikule, "Centrosome control of the cell cycle," *Trends in Cell Biology*, vol. 15, no. 6, pp. 303–311, 2005.

[27] B. Delaval and S. J. Doxsey, "Pericentrin in cellular function and disease," *Journal of Cell Biology*, vol. 188, no. 2, pp. 181–190, 2010.

[28] A. C. Wallace, R. A. Laskowski, and J. M. Thornton, "LIGPLOT: a program to generate schematic diagrams of protein-ligand interactions," *Protein Engineering Design and Selection*, vol. 8, no. 2, pp. 127–134, 1995.

[29] S. Y. Shin, E. Jung, H. Yeo et al., "Design, synthesis, and biological activities of 3-((4, 6-diphenylpyrimidin-2-ylamino) methylene)-2, 3-dihydrochromen-4-ones," *Bioorganic Chemistry*, vol. 120, Article ID 105634, 2022.